

Neutron-diffraction study of stripe order in $\text{La}_2\text{NiO}_{4+\delta}$ with $\delta = \frac{2}{15}$

P. Wochner and J. M. Tranquada

Physics Department, Brookhaven National Laboratory, Upton, New York 11973

D. J. Buttrey

Department of Chemical Engineering, University of Delaware, Newark, Delaware 19716

V. Sachan*

Materials Science Program, University of Delaware, Newark, Delaware 19716

(Received 16 June 1997)

We report a detailed neutron-scattering study of the ordering of spins and holes in oxygen-doped $\text{La}_2\text{NiO}_{4.133}$. The single-crystal sample exhibits the same oxygen-interstitial order but better defined charge-stripe order than that studied previously in crystals with $\delta = 0.125$. In particular, charge order is observed up to a temperature at least twice that of the magnetic transition, $T_m = 110.5$ K. On cooling through T_m , the wave vector ϵ , equal to half the charge-stripe density within an NiO_2 layer, jumps discontinuously from $\frac{1}{3}$ to 0.2944. It continues to decrease with further cooling, showing several lock-in transitions on the way down to low temperature. To explain the observed lock-ins, a model is proposed in which each charge stripe is centered on either a row of Ni or a row of O ions. The model is shown to be consistent with the l dependence of the magnetic peak intensities and with the relative intensities of the higher-order magnetic satellites. Analysis of the latter also provides evidence that the magnetic domain walls (charge stripes) are relatively narrow. In combination with a recent study of magnetic-field-induced effects, we find that the charge stripes are all O centered at $T > T_m$, with a shift towards Ni centering at $T < T_m$. Inferences concerning the competing interactions responsible for the temperature dependence of ϵ and the localization of charge within the stripes are discussed. [S0163-1829(98)00902-3]

I. INTRODUCTION

La_2NiO_4 is a Mott-Hubbard insulator consisting of anti-ferromagnetic NiO_2 planes alternating with La_2O_2 layers. The NiO_2 planes can be doped with holes; however, contrary to conventional expectations, the material remains nonmetallic up to quite large hole concentrations.¹⁻³ There is now considerable evidence that the insulating behavior occurs because the dopant-induced holes tend to order themselves in periodically spaced stripes.⁴⁻¹¹ These charge stripes run diagonally relative to the square lattice defined by the Ni-O-Ni bonds. In the essentially undoped regions between the stripes the Ni spins can order antiferromagnetically, with the charge stripes acting as antiphase domain walls.⁶⁻¹³ This behavior represents an excellent example of "topological" doping in a correlated insulator.¹⁴

In comparing results obtained on samples doped both by Sr substitution and by addition of excess oxygen, several trends have become clear. In samples where both charge and spin orderings have been observed, the charge generally orders at a higher temperature than the spins.^{7,9,11} (The one apparent exception is the case⁶ of $\text{La}_2\text{NiO}_{4+\delta}$ with $\delta = 0.125$. It will be shown in the present paper that, in this composition as well, the charge orders first.) Furthermore, both the charge and spin ordering temperatures increase approximately linearly with the net hole concentration n_h .^{7,9,10} Also varying linearly with n_h is the low-temperature spacing between charge stripes, corresponding to a hole density of roughly one per Ni site along a stripe.

The observed low-temperature hole density within the

stripes is consistent with the mean-field calculations of Zaanen and Littlewood.¹⁵ They evaluated an appropriate three-band Hubbard model at zero temperature and found that electron-phonon couplings tend to reinforce the stability of charged domain walls in an antiferromagnetic background. The numerical calculations yielded a relatively narrow charge stripe centered on a diagonal row of Ni atoms. Zaanen and Littlewood pointed out that the domain-wall states form a half-filled one-dimensional (1D) band, which is unstable to a Peierls distortion. Such a distortion would create a gap at the Fermi level, thus explaining the insulating behavior.

Despite the apparent success of the Hartree-Fock calculations¹⁵ in describing the low-temperature stripe structure, such an approach runs into difficulties at high temperature. In the absence of stripe order, a Hartree-Fock analysis of the doped nickelate would yield a metallic state, whereas numerous studies¹⁶⁻²¹ have shown that even above the charge-ordering temperature the optical conductivity is dominated by midinfrared absorption bands, with no $\omega = 0$ Drude component. Furthermore, neutron-diffraction studies of the ordered state have shown that in some cases the stripe spacing changes with temperature,^{6,9} implying a variation in the charge density within a stripe. Thus, one cannot rely on a unique stripe charge density to explain the insulating behavior.

It is clear that there are mysteries remaining to be unraveled. For example, what is the nature of the temperature-dependent variation of the stripe spacing? How narrow are the charge stripes, and to what extent are they pinned to the

lattice? Are charge stripes actually centered on Ni rows, or are other configurations possible? To address these issues, a well-ordered sample is required.

Much of the work cited above has focused on Sr-doped La_2NiO_4 . That system has the advantage of allowing a continuous variation of the hole concentration by dopants whose random positions are fixed at relatively high temperature. The down side is that the disorder of the dopants appears to prevent the development of long-range stripe order.^{4,7,9,11} The alternative is to study oxygen-doped $\text{La}_2\text{NiO}_{4+\delta}$. The constraint here is that one must work with the phases that nature provides: ordered phases occur only at special values of δ , and for an arbitrary value of δ one may observe phase separation.^{8,10,22-27} On the positive side, long-range order of interstitials and charge stripes coincide in a composition originally characterized as $\delta=0.125$.^{6,8,10,28}

Analysis of neutron-diffraction measurements on one particular $\delta=0.125$ crystal⁸ indicated that the ordered interstitial structure actually corresponds to an ideal oxygen excess of $\delta=\frac{2}{15}=0.133$. Thus, the $\delta=0.125$ composition is oxygen deficient relative to the ideal phase. As will be explained below, we have prepared a new crystal that appears to correspond much more closely to the ideal value of δ . The magnetic Bragg peaks measured on this crystal are sharper than those observed with the $\delta=0.125$ crystal,^{6,8} thus allowing better sensitivity to the features of interest. We have recently reported results on magnetic-field-induced staggered magnetization²⁹ and on spin excitations in the stripe-ordered phase³⁰ measured on the same crystal. In the present paper we concentrate on various aspects of the static stripe order in zero field.

In earlier studies^{6,28} of $\delta=0.125$ crystals, an apparently discontinuous jump from zero to finite intensity of both the magnetic and charge-order superlattice peaks was observed on cooling below $T_m=110.5$ K. With the $\delta=0.133$ crystal we observe a similar discontinuous jump in the intensities, but we find that charge order clearly survives at $T>T_m$ with a jump in the stripe spacing to a value commensurate with a second harmonic of the interstitial order. In the latter regime the charge-order peak intensity decreases exponentially with temperature, so that no clear transition to the disordered state has been observed.

To obtain a more precise measure of the incommensurate splitting ϵ of the magnetic peaks at $T<T_m$, we measured the temperature dependence of the position and intensity of a third-harmonic peak. Where previous work⁶ had provided weak evidence that ϵ , which varies with temperature, tends to show lock-in behavior at certain rational fractions, the present results show clear plateaus at $\epsilon=\frac{2}{7}$ ($98\text{ K}\leq T\leq 102\text{ K}$) and $\epsilon=\frac{5}{18}$ ($75\text{ K}\leq T\leq 92\text{ K}$). The lock-ins demonstrate that the charge stripes are coupled to the lattice. To explain the continuous distribution of ϵ values found at other temperatures, an analogy is made with the problem of finding the ground-state arrangement of integral charges on a one-dimensional lattice at arbitrary filling. From the solution^{31,32} to the latter problem, it appears that a devil's staircase of ordered phases should be possible; however, due to entropy, long-range order is observed only for phases with relatively short periods. The fact that ϵ varies with temperature indicates that competing interactions must be involved in determining the order.⁹

Coupling to the lattice is also evident in the way that the stripes align themselves from one layer to the next. If there were no interaction with the lattice (as was assumed previously⁸), then the stripes within a layer would be uniformly spaced, and their positions would be staggered from one layer to the next in order to minimize the Coulomb energy. Such a symmetric stacking of the layers of stripes can lead to forbidden superlattice peaks corresponding to the charge order, similar to the situation for nuclear reflections due to the average body-centered stacking of the NiO_2 layers. However, the pinning of the charge stripes to the lattice means that the shift of the stripe pattern from one layer to the next can only occur in increments of the lattice spacing. As a consequence, the intensities of the magnetic peaks oscillate as a function of the component of the momentum transfer that is perpendicular to the planes. We show that the modulation of the intensities can be modeled quantitatively in terms of the stacking structure factor when a small amount of stacking disorder is taken into account. It follows that the missing charge-order peaks are not forbidden, but just extremely weak.

To characterize the widths of the charge stripes, we have measured the higher harmonic magnetic Bragg peaks. Narrow domain walls give squared-off magnetic domains, and deviations from a sinusoidal modulation are reflected in finite Fourier components beyond the first harmonic. Another contribution to the higher harmonics can come from an alternation of the stripe spacing associated with the pinning to the lattice. We show that although the intensities of the higher harmonics are all quite weak, with the strongest (the third) being $<2\%$ of the first, they are consistent with narrow charge stripes. Furthermore, the weakness of the harmonics in the case of $\epsilon=\frac{2}{7}$ indicates that stripes can be centered both on rows of Ni atoms and on rows of O atoms. Assuming that the stripes are Ni centered at low temperature, the temperature dependence of ϵ implies that the stripes become O centered at high temperature. This leads to a prediction of ferrimagnetic correlations in the stripe-ordered regime at $T>T_m$, which was recently confirmed by measurements in a magnetic field.²⁹

The rest of the paper is organized as follows. The next section contains a description of experimental procedures, and it is followed by a brief review of nomenclature and notation. The temperature dependences of the intensities and positions of superlattice peaks are presented and analyzed in Sec. IV. The results relevant to interlayer stacking of stripes are treated in Sec. V. In Sec. VI the intensities of the magnetic higher harmonic satellites are analyzed. The significance of these results is discussed in Sec. VII, and a brief summary is given in Sec. VIII.

II. EXPERIMENTAL PROCEDURES

The single-crystal sample used in the present study was grown by radio-frequency skull melting as described elsewhere.²⁴ The oxygen concentration was selected by annealing at 464°C for 5 days in flowing O_2 (1 bar) followed by a quench to room temperature. The annealing conditions were chosen to give a nominal δ of 0.150, based on earlier work on the phase diagram.²⁴ An initial neutron-diffraction study of this crystal in 1993 indicated that the dominant

oxygen-ordered phase is the same as that found previously⁸ in a crystal with $\delta=0.125$. There were also weak diffraction peaks indicative of a second phase with a different δ ; however, these were absent ~ 1.5 years later when the present study was initiated. (One fact that might be relevant to the disappearance of the second phase is that the crystal was stored in a He atmosphere, which is relatively reducing, rather than in air.) The room-temperature lattice parameters obtained at that later time are $a=5.461 \text{ \AA}$ and $c=12.674 \text{ \AA}$. Making use of the calibration established by the earlier x-ray diffraction study,²⁴ the c/a ratio of 2.3208 indicates $\delta=0.136\pm 0.005$, consistent with the ideal value of $\frac{2}{15}$ for the model ordered interstitial structure identified⁸ in the case of $\delta=0.125$.

The neutron-diffraction measurements were performed on the H4M, H8, and H9A triple-axis spectrometers at the High Flux Beam Reactor located at Brookhaven National Laboratory. At H9A, which is on the cold source, neutrons of energy 5.0 meV were selected. Effective horizontal collimations of 40'-40'-20'-40' (from reactor to detector) were used together with a cold Be filter to eliminate neutrons at shorter harmonic wavelengths. At H4M and H8 a neutron energy of 14.7 meV, horizontal collimations of 40'-40'-40'-40' or 40'-40'-80'-80' and a pyrolytic graphite (PG) filter were used. At all spectrometers the neutrons were monochromatized and analyzed by PG crystals set for the (002) reflection.

The cold neutrons at H9A were used to study the weak higher-order satellites of the magnetic-scattering peaks, which are strongest at small momentum transfer \mathbf{Q} . The excellent signal-to-background ratio of H9A together with the larger scattering angles in the case of cold neutrons compared to higher energy neutrons enabled the determination of third-order satellite positions with high precision. The higher-energy neutrons at H4M and H8 were required to measure the nuclear scattering associated with lattice displacements due to charge order. Except for the third-harmonic measurements, where scans were taken along $Q=(h,0,1)$, integrated intensities were determined from $\theta-2\theta$ scans.

All measurements were performed with the crystal oriented so that the $(h,0,l)$ zone of reciprocal space was in the horizontal scattering plane. (The notation and choice of unit cell are explained in the following section.) The aligned crystal was mounted in an Al can filled with He exchange gas that was attached to the cold finger of a Displex closed-cycle refrigerator. The temperature was measured with a Si diode and a Pt resistance thermometer to an accuracy of better than ± 1 K.

The ordering kinetics of the oxygen interstitials can be rather slow, and the cooling rate through the ordering transition can affect whether long-range order is achieved. For example, extremely slow cooling is required to optimize the order in the case³³ of $\delta=0.105$, and rapid cooling also had measurable effects in studies^{8,10} of $\delta=0.125$. In the present case, no significant effects of cooling rate on interstitial order were observed. On the other hand, the cooling and heating history for $T\leq T_m$ has an influence on the relative fractions of coexisting magnetic phases, the width of the temperature regions where the magnetic wave vector is locked-in to rational fractions, and the detailed spectral weight of higher

order magnetic satellites and their peak widths. Therefore, the temperature dependence was studied during slow, careful warming after an initial cool down to 10 K.

III. NOTATION

In order to describe and explain the data it is first necessary to review the structure⁸ and explain our notation. Within the resolution of our instrument, the fundamental reflections of this crystal indicate a tetragonal symmetry (space group $I4/mmm$) down to at least 10 K, whereas the structural superlattice peaks suggest an orthorhombic symmetry. To describe the diffraction peaks we will use an indexing based on an orthorhombic cell (or pseudotetragonal $F4/mmm$) with a unit-cell size $\sqrt{2}a_t \times \sqrt{2}a_t \times c_t$ relative to the basic body-centered-tetragonal cell. Note that in the body-centered-tetragonal cell the a and b axes are parallel to the Ni-O bonds within the NiO_2 planes, whereas in the larger cell that we use the axes are rotated from the bonding directions by 45° .

Four different types of superlattice peaks can be found in this sample. Two of them correspond to the ordering of the oxygen interstitials and the other two involve ordering of the doped holes and the Ni spins. Each set of peaks is characterized by a wave vector \mathbf{g}_j such that \mathbf{Q}_{SL} , the position of a superlattice peak of type j , is given by

$$\mathbf{Q}_{SL} = \mathbf{G} \pm \mathbf{g}_j, \quad (1)$$

where \mathbf{G} is a reciprocal-lattice vector corresponding to the average pseudotetragonal unit cell. The oxygen order is characterized by two wave vectors,

$$\mathbf{g}_{O(1)} = \left(\frac{1}{3}, 0, 1 \right) \quad (2)$$

and

$$\mathbf{g}_{O(2)} = \left(0, \frac{4}{5}, \frac{4}{5} \right), \quad (3)$$

where wave-vector components are specified in reciprocal-lattice units of $(2\pi/a, 2\pi/a, 2\pi/c)$. The twinning associated with the interstitial order is described in Ref. 8.

To describe the superlattice peaks associated with stripe order it is necessary to expand the set of reciprocal-lattice vectors considered in Eq. (1). The symmetry relationship between the two NiO_2 planes per $F4/mmm$ unit cell leads to forbidden reflections. For example, for reciprocal lattice vectors of the type $(H,0,L)$ one has the requirements that both H and L be even integers. We will show in Sec. V that the stripe patterns in neighboring layers are *not* related by symmetry, and as a result the relevant reciprocal-lattice vectors include the case where L is odd.

The positions of the magnetic and charge-order superlattice peaks within the $(h,0,l)$ zone are illustrated in Fig. 1(a). The charge order is determined by

$$\mathbf{g}_{2\epsilon} = (2\epsilon, 0, 0), \quad (4)$$

with the average distance between domain walls in real space equal to $a/2\epsilon$. The magnetic order involves two modulation

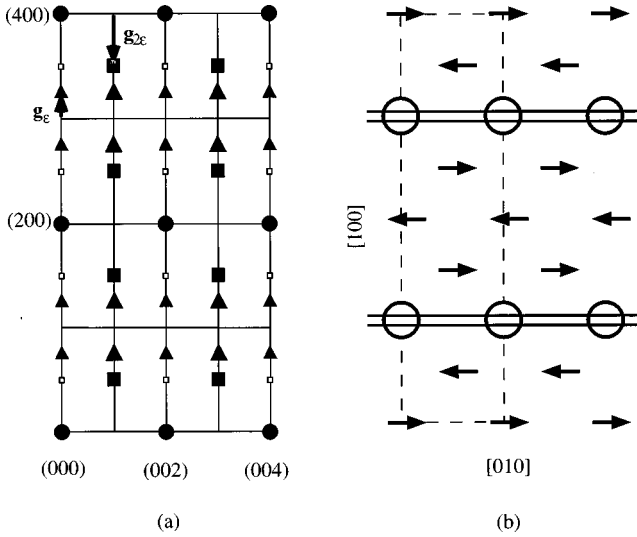


FIG. 1. (a) Diagram of the $(h0l)$ zone, showing positions of diffraction peaks, with indexing based on space group $F4/mmm$ for the average nuclear structure. Solid circles, fundamental Bragg peaks; solid triangles, magnetic superlattice peaks; solid squares, nuclear superlattice peaks corresponding to charge order; open squares, allowed but unobserved charge-order peak positions. Oxygen ordering peaks are excluded. (b) Model of spin and hole ordering in a NiO_2 plane, as discussed in the text; circles indicate positions of holes (Ni centered), arrows indicate correlated Ni moments. The dashed line outlines a unit cell, and double lines mark positions of domain walls.

wave vectors. Simple antiferromagnetic order would be described by $\mathbf{g} = \mathbf{Q}_{\text{AF}} = (1,0,0)$. Stripe order results in a second modulation

$$\mathbf{g}_\epsilon = (\epsilon, 0, 0), \quad (5)$$

so that the net wave vector is $\mathbf{g} = \mathbf{Q}_{\text{AF}} \pm \mathbf{g}_\epsilon$. In real space the spin structure consists of locally antiferromagnetic order with an overall modulation period a/ϵ , twice that of the charge period, reflecting the fact that the hole stripes act as antiphase boundaries for the spin structure. The idealized real-space spin and charge structure for $\epsilon = \frac{1}{4}$ is presented in Fig. 1(b).

Of course, \mathbf{g}_ϵ and $\mathbf{g}_{2\epsilon}$ represent only the dominant sinusoidal components of the magnetic and charge-order modulations, respectively. Deviations from sinusoidal modulations will result in superlattice peaks corresponding to higher Fourier components of the order. The modulation wave vector for the n th harmonic is simply

$$\mathbf{g}_{n\epsilon} = (n\epsilon, 0, 0). \quad (6)$$

For the magnetic scattering, only harmonics with n odd will appear, split about \mathbf{Q}_{AF} . (The absence of magnetic harmonics with n even follows directly from the antiphase nature of the order.) Harmonics with n even correspond to charge order.

IV. TEMPERATURE DEPENDENCE OF STRIPE ORDER

A. Experimental results

The overall temperature dependence of the stripe order is best characterized by looking at first- and second-harmonic

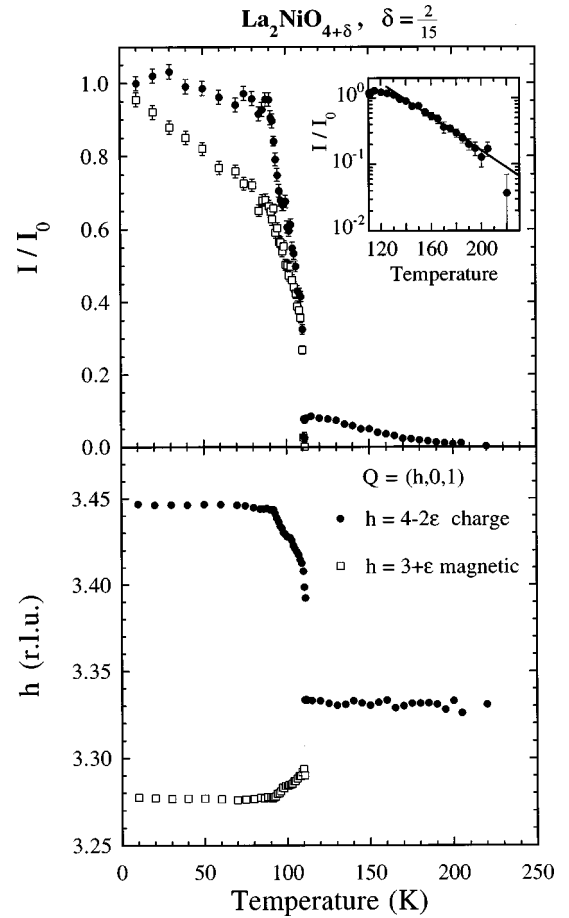


FIG. 2. Temperature dependences of a magnetic peak at $(3 + \epsilon, 0, 1)$ (open squares) and a charge-order peak at $(4 - 2\epsilon, 0, 1)$ (filled circles). The upper panel shows integrated intensities normalized with respect to 10 K, the lower gives the peak position in h . Inset: logarithm of normalized intensity vs temperature for the charge-order peak above 110 K. Line through points is a linear fit, as discussed in the text.

peaks. Figure 2 presents results for a magnetic superlattice peak at $(3 + \epsilon, 0, 1)$ and a charge-order peak at $(4 - 2\epsilon, 0, 1)$. The upper panel shows the integrated peak intensity normalized with respect to 10 K, while the lower gives the peak position h measured in a $[h, 0, 0]$ scan. As found previously,^{6,28} cooling through $T_m = 110.5$ K results in a discontinuous jump in intensity of both the magnetic and charge-order peaks, with a concomitant temperature dependence of the peak positions. The new feature that we have to report is a peak at $\epsilon = \frac{1}{3}$ for $T \geq T_m$. Scattering at this position could come from either magnetic or charge order (or both); however, the \mathbf{Q} dependence of the structure factor indicates that it corresponds uniquely to charge order. (The intensity of $\epsilon = \frac{1}{3}$ peaks disappears at small Q , where the magnetic form factor is largest.)

The discontinuity of the transition at T_m is illustrated in Fig. 3. At a temperature 0.5 K below the transition we observe one peak due to magnetic order and another corresponding to charge order. Right at T_m a third peak appears at $\epsilon = \frac{1}{3}$, coexisting with the previous two. At 0.5 K above T_m only the $\epsilon = \frac{1}{3}$ charge-order peak survives. In contrast to the behavior at $T < T_m$, the position of the peak remains locked at $\epsilon = \frac{1}{3}$ while its intensity gradually decreases with increasing temperature.

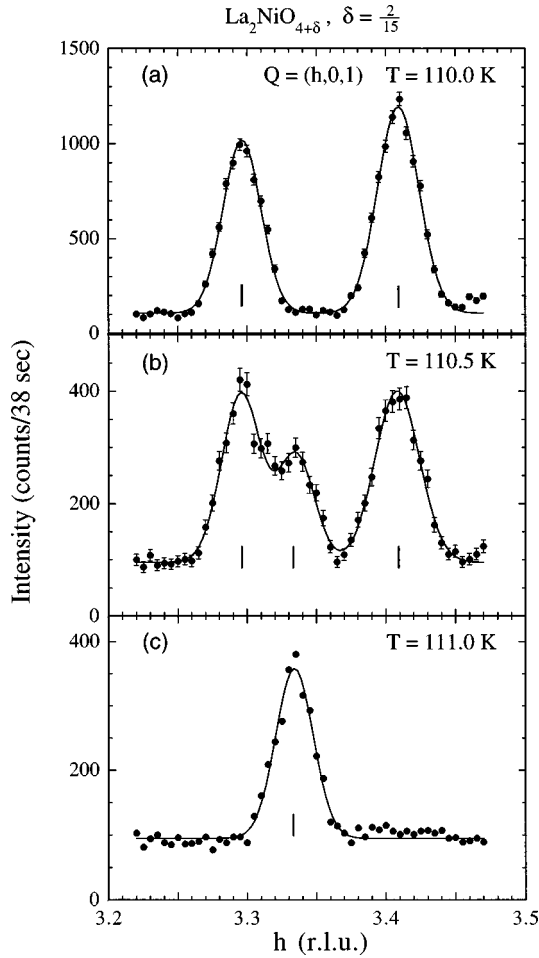


FIG. 3. Elastic scans along $\mathbf{Q}=(h,0,1)$. Scans were measured at temperatures of 110 K (a), 110.5 K (b), and 111 K (c).

The temperature dependence of the $\epsilon=\frac{1}{3}$ peak is presented on a logarithmic scale in the inset of Fig. 2. The linear variation of the intensity for $T \geq 150$ K is analogous to a Debye-Waller-like behavior with

$$I \sim e^{-2T/T_0}, \quad (7)$$

and $T_0 = 67 \pm 5$ K. Such a temperature dependence is in sharp contrast to the usual critical behavior associated with an order-disorder transition. In connection with this, it is useful to note that

$$\mathbf{g}_{2\epsilon} = \left(\frac{2}{3}, 0, 0 \right) \equiv 2\mathbf{g}_{0(1)}, \quad (8)$$

so that there is a type of commensurability between the charge stripes in the planes and the interstitial order along one direction of the lattice. The Debye-Waller-like decay of the intensity suggests that the charge correlations are fluctuating about an average ordered configuration determined by the ordered interstitial oxygens. It is possible that the charge order does not entirely disappear until the interstitials disorder.

The ordering of the spins at T_m is associated with jumps both in the charge-order intensity and in ϵ . Previously⁶ it was found that the superlattice peak intensities show simple power-law correlations with the quantity

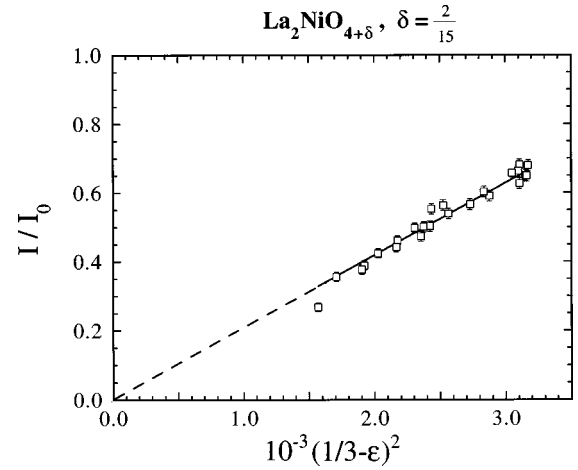


FIG. 4. Normalized intensity of a magnetic peak at $(3+\epsilon, 0, 1)$ vs $(1/3-\epsilon)^2$ for $80 \text{ K} \leq T \leq T_m$. Line through points is a linear fit, as discussed in the text.

$$q = \frac{1}{3} - \epsilon. \quad (9)$$

From the measurements between T_m and 80 K, we find for the magnetic-peak intensity that

$$I_{\text{mag}} \approx aq^2, \quad (10)$$

as illustrated in Fig. 4. This result is completely empirical, as there is no theoretical prediction for the connection between the intensity and wave vector.

A prediction does exist for the relationship between the intensities of the magnetic and charge order peaks below T_m . Zachar, Kivelson, and Emery³⁴ have solved an appropriate Landau model for coupled charge- and spin-density-wave order parameters, ρ and S , respectively. They find that when the charge is the first to order, it is possible to have a first-order transition when the spins order, as we observe. At temperatures below the magnetic transition, the relationship between the order parameters is predicted to be, to lowest order,

$$\rho - \rho_0 = A|S|^2, \quad (11)$$

where A is a constant and ρ_0 denotes the magnitude of ρ just above the magnetic transition temperature. Since the intensities of the magnetic and charge-order peaks are related to the order parameters by $I_{\text{mag}} \sim |S|^2$ and $I_{\text{ch}} \sim |\rho|^2$, Eq. (11) implies that, for $T < T_m$,

$$[I_{\text{ch}}(T)]^{1/2} - [I_{\text{ch}}(T_m^+)]^{1/2} = A' I_{\text{mag}}(T) \equiv \Delta I_{\text{ch}}^{1/2}, \quad (12)$$

where $I_{\text{ch}}(T_m^+)$ is the intensity of the charge-order peak at a temperature just above T_m . Keeping in mind that the model does not describe the temperature dependence of the wave vector, so that there may be missing correction terms, we show in Fig. 5 that this relationship is at least plausible near the transition.

The steplike structures in the lower panel of Fig. 2 are suggestive of lock-in transitions. To obtain more precise measurements of ϵ versus temperature, we studied a third-harmonic magnetic peak, $(1-3\epsilon, 0, 1)$. This reflection occurs at a relatively low scattering angle, and a scan through the

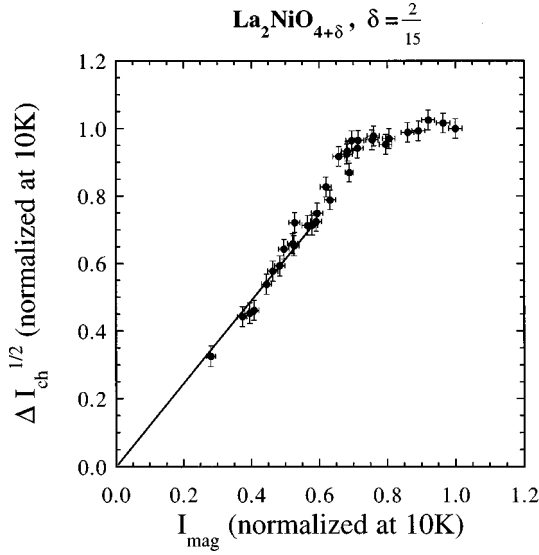


FIG. 5. Intensity of the $(4-2\epsilon, 0, 1)$ charge-order peak, plotted in the form $\Delta I_{\text{ch}}^{1/2}(T)$ and normalized to the 10-K value, vs the normalized $(3+\epsilon, 0, 1)$ intensity.

peak along the $[h, 0, 0]$ direction is nearly transverse to \mathbf{Q} . For such conditions the resolution in h is excellent. In our case the resolution was limited by the sample mosaic ($\approx 0.7^\circ$). At many temperatures the peak shape and width are limited by the asymmetric mosaic distribution of the sample. Representative scans are shown in Fig. 6. At other temperatures we observed either a single broadened peak, or the coexistence of a broadened peak and a mosaic-limited one.

A summary of the results is given in Fig. 7. In all panels, the dominant component is represented by the filled symbols and the secondary component by the open ones. (The exception to this rule occurs in the range between 50 and 70 K, where the integrated intensity of the broader second component is actually greater than that of the sharper peak.) The top panel shows the integrated intensity, with the total intensity from both components (dashed line) normalized to one at 10 K. The middle panel and inset show ϵ . The bottom panel gives the peak width, divided by 3 (in units of $2\pi/a$), so that it can be compared directly with the middle panel.

The temperature dependence of ϵ is rather interesting. Although it was measured on warming, it is more convenient to discuss the behavior starting from T_m and considering the changes as the temperature decreases. (Hysteresis effects should be small as long as one cools sufficiently slowly.) Initially, ϵ jumps from $\frac{1}{3}$ to $0.2944 \approx \frac{5}{17}$. From there it decreases linearly with temperature until it hits a plateau at $0.286 = \frac{7}{24}$. (There is also a hint of a plateau at $0.293 = \frac{12}{41}$, although the stability of this particular value is surprising, as discussed below.) The $\frac{7}{24}$ plateau extends from 102 down to 98 K. Below this, ϵ jumps to another region of linear decrease, until it locks into a value of $0.2778 = \frac{5}{18}$ near 93 K. From this point down to 10 K a $\frac{5}{18}$ component is always present; however, the entire system is locked into this value only down to ~ 75 K. Near 70 K the third harmonic splits into two peaks: a sharp one at $\frac{5}{18}$ and a broad one centered near 0.275. The integrated intensity of the broad peak dominates down to ~ 50 K, below which most of the intensity shifts back into the sharp $\frac{5}{18}$ peak. In contrast to what was

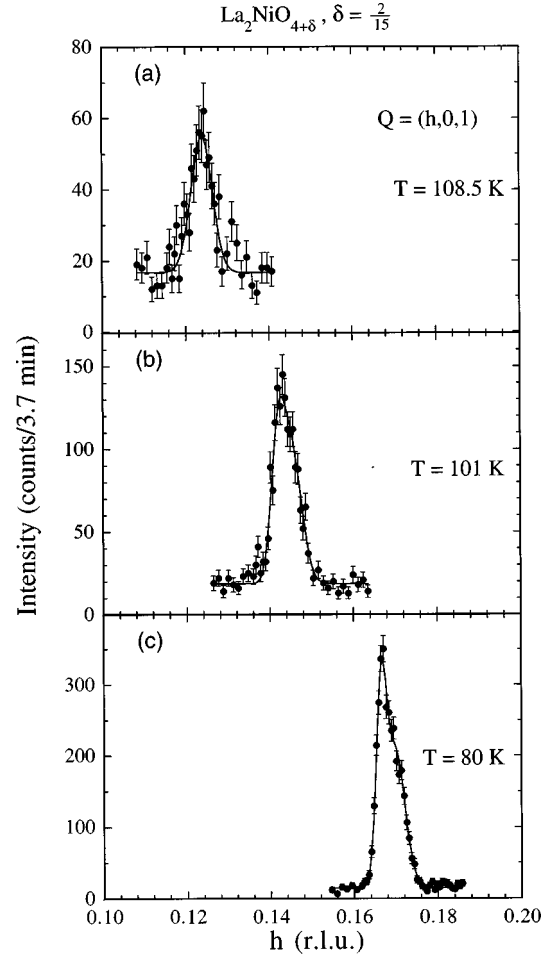


FIG. 6. Elastic scans along $\mathbf{Q}=(h, 0, 1)$. Scans were measured at temperatures of 108.5 K (a), 101 K (b), and 80 K (c).

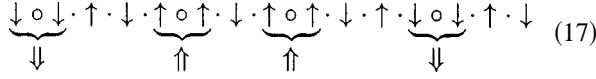
found⁶ with the $\delta=0.125$ crystal, we have not observed any component centered at $\frac{3}{11} = 0.2727$.

B. Analysis

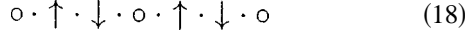
In order to make sense of $\epsilon(T)$, we can start with the Zaanen and Littlewood¹⁵ prediction of charge stripes with a hole density of one per Ni site. Assuming that all dopant-induced holes go into O $2p$ states lying within the NiO_2 layers, one would then expect a domain-wall density of $\epsilon = 2\delta$ per row of nickel atoms. In our case this gives $\epsilon = \frac{4}{15} = 0.267$. It appears that the measured ϵ is approaching this value as the temperature decreases, but it never quite gets there. If we assume that all of the holes are indeed ordered in the stripes, then the hole density (per Ni site) within a charge stripe, n_s , is given by $n_s = 2\delta/\epsilon$. Even if all holes remain confined to the stripes as the temperature is raised, the fact that ϵ increases implies that n_s is decreasing. At 80 K we have $n_s = 0.960$, at 100 K $n_s = 0.933$, and at $T \geq T_m$ $n_s = 0.800$.

The existence of plateaus in $\epsilon(T)$ indicates that the stripe order can couple to the lattice; however, the almost continuous variation of ϵ between plateaus shows that the stripe density is not restricted to a few special values. To describe the possible stripe arrangements, we need consider only the one-dimensional ordering along the charge-modulation di-

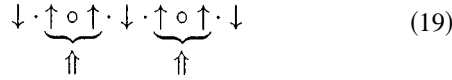
or purely O-centered stripes:



In the single-spacing phase $\epsilon = \frac{1}{3}$, Ni-centered stripes give



while O-centered stripes yield



For our $\delta=0.133$ crystal, the magnetic order vanishes when ϵ shifts to $\frac{1}{3}$; nevertheless, inelastic-scattering measurements show that the spins remain correlated.³⁰ In the configuration with O-centered stripes, the domain walls have moments that are in phase with each other. As will be discussed further in Sec. VI, one might expect the moments of Ni ions immediately adjacent to an O-centered domain wall to be somewhat reduced compared to those in the middle of a magnetic domain. If the modulation of the moments defining the antiphase domains were purely sinusoidal, then there would be no net moment in the system; however, any deviation from a pure sine wave would lead to ferrimagnetism. In contrast, the spins all form antiparallel pairs when the stripes are centered on Ni rows. Recently we demonstrated²⁹ that one can induce staggered magnetic order in the $\epsilon = \frac{1}{3}$ phase by applying a uniform magnetic field. This result clearly indicates that the stripes in the high-temperature phase are centered on O rows.

So far we have considered only phases with uniform stripe spacing, whereas the real system appears to pass through a range of more complicated phases. While we have emphasized the possibility of two types of charge stripes, it is important to note that the observed values of ϵ can be explained with a single type of stripe. In that case, the relevant phases of uniform spacing are limited to $\epsilon = \frac{1}{4}$ and $\frac{1}{3}$. To describe the possible intervening phases it is convenient to introduce a simple notation. First note that for $\epsilon = \frac{1}{4}$, there is one spin period in four lattice spacings, or, equivalently, one charge stripe per four rows of Ni atoms (with two rows per fundamental unit cell). It follows that this phase can be denoted in terms of the real-space repeat unit of the charge stripes as $\langle 4 \rangle$. Similarly, $\epsilon = \frac{1}{3}$ corresponds to $\langle 3 \rangle$. The configuration $\langle 43 \rangle$ represents alternating stripe spacings of four Ni rows and three Ni rows. This corresponds to two stripes per seven Ni rows, or $\epsilon = \frac{2}{7}$. An arbitrary configuration will consist of n four-row spacings and m three-row spacings, giving⁶

$$\epsilon = \frac{n+m}{4n+3m}. \quad (20)$$

For such an arbitrary configuration, the ground-state energy is minimized by arranging the stripes in a pattern that is as

TABLE I. Some of the more stable stripe configurations in the range $\frac{1}{4} < \epsilon < \frac{1}{3}$ assuming a single type of charge stripe. The notation is explained in the text.

n	m	ϵ		Configuration
		Fraction	Decimal	
2	1	$\frac{3}{11}$	0.2727	$\langle 443 \rangle$
5	3	$\frac{8}{29}$	0.2759	$\langle 44344343 \rangle$
3	2	$\frac{5}{18}$	0.2778	$\langle 44343 \rangle$
1	1	$\frac{2}{7}$	0.2857	$\langle 43 \rangle$
2	3	$\frac{5}{17}$	0.2941	$\langle 43343 \rangle$

close to uniform as possible.^{31,35} Some examples are shown in Table I. Bak and Bruinsma³² have demonstrated that the possible ground states form a complete Devil's staircase.

Of course, if two types of stripes are considered, then we must include a possible stripe spacing of $\frac{7}{2}$ Ni rows. Note that to be commensurate with the Ni-row spacing such units must occur in pairs. Let the number of pairs of $\frac{7}{2}$ spacings per real space repeat unit be p . Then, in the range $\frac{1}{4} \leq \epsilon \leq \frac{2}{7}$, the values of ϵ are given by

$$\epsilon = \frac{n+2p}{4n+7p}, \quad (21)$$

while, in the range $\frac{2}{7} \leq \epsilon \leq \frac{1}{3}$, the appropriate formula is

$$\epsilon = \frac{2p+m}{7p+3m}. \quad (22)$$

Examples are shown in Table II.

One can distinguish between models with either one or two types of stripes by analyzing the intensities of higher harmonic satellites. Such an analysis is discussed in Sec. VI. The proposed pinning of the stripes to particular lattice rows has implications for the layer to layer stacking of the stripes, as we discuss in the next section.

V. STACKING OF STRIPES

To minimize the Coulomb repulsion between charge stripes in neighboring planes, the stripes should run parallel to each other with a staggered alignment. Such a body-centered-type arrangement would maximize the spacing be-

TABLE II. Some of the more stable stripe configurations in the range $\frac{1}{4} < \epsilon < \frac{1}{3}$ assuming two types of stripes. The notation is explained in the text.

n	p	m	ϵ		Configuration
			Fraction	Decimal	
1	1	0	$\frac{3}{11}$	0.2727	$\langle 4 \frac{7}{2} \frac{7}{2} \rangle$
2	3	0	$\frac{8}{29}$	0.2759	$\langle 4 \frac{7}{2} \frac{7}{2} \frac{7}{2} 4 \frac{7}{2} \frac{7}{2} \frac{7}{2} \rangle$
1	2	0	$\frac{5}{18}$	0.2778	$\langle 4 \frac{7}{2} \frac{7}{2} \frac{7}{2} \frac{7}{2} \rangle$
0	1	0	$\frac{2}{7}$	0.2857	$\langle \frac{7}{2} \frac{7}{2} \rangle$
0	2	1	$\frac{5}{17}$	0.2941	$\langle \frac{7}{2} \frac{7}{2} \frac{7}{2} \frac{7}{2} 3 \rangle$

TABLE III. Examples of $|F|^2$ for both magnetic and charge-order peaks in the case of body-centered stacking of stripe-ordered layers.

ϵ	$ F(1 \pm \epsilon, 0, l) ^2$		$ F(3 \pm \epsilon, 0, l) ^2$		$ F(2 \pm 2\epsilon, 0, l) ^2$		$ F(4 \pm 2\epsilon, 0, l) ^2$	
	l even	l odd	l even	l odd	l even	l odd	l even	l odd
$\frac{1}{4}$	2	2	2	2	0	4	0	4
$\frac{3}{11}$	0	4	4	0	4	0	0	4
$\frac{5}{18}$	2	2	2	2	0	4	0	4
$\frac{2}{7}$	2	2	2	2	0	4	4	0
$\frac{1}{3}$	4	0	0	4	4	0	0	4

tween nearest neighbors; however, pinning of the stripes to the lattice would prevent such an ideal staggering. Within our model, the stripe pattern should only be able to shift by integral (or possibly half integral) units of the lattice spacing a . We can distinguish between these two possibilities, symmetric versus integral-shift stacking, by analyzing the l dependence of the superlattice intensities.

Consider first the case of a symmetric, body-centered stacking of the stripes. As discussed in the previous section, a given value of ϵ can be written as a ratio of two integers, r/s . The commensurate period of the magnetic structure is then sa , and the period of the charge structure is $sa/2$. The displacement of the stripe pattern from one layer to the next is then $(\frac{1}{4}s, 0, \frac{1}{2})$, in lattice units. The structure factor describing such a stacking is

$$F = 1 + e^{i\pi(1/2)sh+l}, \quad (23)$$

where the intensity is proportional to $|F|^2$. For a charge-order reflection of the type $(2n+2\epsilon, 0, l)$, where n is an integer, $|F|^2$ is either 4 or 0. In the case of $\epsilon = \frac{1}{4}$, one finds that $|F|^2$ is equal to 0 for l equal to an even integer and 4 for odd l , independent of n . For the general case of $\epsilon = r/s$, however, the value of $|F|^2$ depends not only on l , but also on r , s , and n . There is a similar variability for magnetic reflections. To illustrate this, we have listed values of $|F|^2$ for a number of different cases in Table III. Note in particular that the body-centered-stacking model implies zero intensity for the $(4-2\epsilon, 0, 1)$ reflection when $\epsilon = \frac{2}{7}$, which is clearly inconsistent with the results shown in Fig. 2. (The tabulated values of $|F|^2$ for $\epsilon = \frac{1}{3}$ have implications for the interpretation of magnetic and charge-order scattering as reported in a recent study¹¹ of $\text{La}_{1.67}\text{Sr}_{0.33}\text{NiO}_4$.)

Alternatively, if the stripes are pinned to the lattice, then the stripe order in neighboring layers is described by the basis vectors $(0, 0, 0)$ and $(ma, 0, c/2)$, where m is an integer number. Taking the simplest case of $m = 1$, one finds that, for the n th harmonic superlattice peak,

$$|F_n|^2 = 2[1 + (-1)^l \cos(2\pi n\epsilon)]. \quad (24)$$

This formula indicates that, for fixed h , the intensities of magnetic peaks should oscillate as a function of l . It turns out that this is just what is observed.

We measured integrated intensities for ten first-harmonic peaks at $(1 \pm \epsilon, 0, l)$, with $l = 0$ to 4, at the 80 and 100 K plateaus, corresponding to $\epsilon = \frac{5}{18}$ and $\frac{2}{7}$, respectively. To describe the experimental results, it is helpful to express the integrated intensities of the $n = 1$ magnetic reflections as

$$I_1(l) = Af^2|F_1|^2, \quad (25)$$

where A is a normalization constant, and we use the parametrization $f = e^{-Q^2/2\sigma^2}$ to approximate the Ni magnetic form factor as well as the Debye-Waller factor. The parameter σ was determined by a least-squares fit to the data. The values of $|F_1|^2$ extracted from the 80 K measurements are shown in Fig. 8. The dominant l dependence of these results is described by the formula

$$|F_n|^2 = A'[1 + (-1)^l B_n], \quad (26)$$

where we have kept the notation general by labeling F and B with n , and the scale factor A' is meant to remind us that we have not determined from the experimental intensities the absolute magnitude of $|F_1|^2$. The values of B characterizing the measurements at 80 and 100 K are listed in Table IV. Equation (24) predicts that $B_1 = \cos(2\pi\epsilon)$, which yields $B_1 = -0.174$ at 80 K ($\epsilon = \frac{5}{18}$), and $B_1 = -0.223$ at 100 K ($\epsilon = \frac{2}{7}$).

The model allowing an interlayer offset of the stripe pattern by one lattice spacing gives qualitative agreement with experiment, although the calculated magnitude of the parameter B_1 appears to be systematically too large by 30%. We can get a better fit to the data if we allow for some disorder in the stacking in terms of different offsets. The Coulomb energy between charge stripes in neighboring layers is not the same for all possible integral offsets. If we allow for two possible offsets, a and ma , with relative probabilities $1 - \alpha$ and α , respectively, then, assuming a random distribution of the offsets, the structure factor becomes

$$F_n = 1 + [(1 - \alpha)e^{-i2\pi n\epsilon} + \alpha e^{-i2\pi m\epsilon}]e^{-i\pi l}. \quad (27)$$

In the $\frac{5}{18}$ phase, the Coulomb energy is minimized for $m = 1$, and also for $m = 8$. We fit the measured intensities with this model, varying the parameters α and σ to obtain the

TABLE IV. Values of the l -dependent coefficient B_n (described in the text) for harmonics $n = 1-4$. For $n = 1$, experimental and fitted values are given. For $n = 3$, experimental values are compared with values calculated using the parameters determined from the $n = 1$ fit. Only calculated values are given for $n = 2$ and 4.

T (K)	B_1		B_3		B_2	B_4
	Expt.	Fit	Expt.	Calc.	Calc.	Calc.
80	-0.13(1)	-0.132	0.34(7)	0.398	-0.964	0.841
100	-0.15(1)	-0.153	0.54(2)	0.508	-0.854	0.508

TABLE V. Fitted values of the occupation fraction α for layers with basis vector $(ma, 0, c/2)$ in the average magnetic unit cell and σ , the Ni magnetic form-factor constant. $R_w = \sum w_n^2 (I_{\text{obs}} - I_n)^2 / \sum w_n^2 I_{\text{obs}}^2$; $w_n =$ statistical weight.

T	ϵ	m	α	σ	R_w
80 K	$\frac{5}{18}$	8	0.123(2)	3.2(2)	0.034
100 K	$\frac{2}{7}$	3	0.1182(2)	3.1(2)	0.035

results shown in Fig. 8. The parameter values and the weighted reliability factor R_w are listed in Table V. For $\frac{2}{7}$, the relevant offsets are $m=1$ and 3 (with a shift by $2.5a$ being equivalent in energy to $m=1$). Again, the fitting results are listed in Table V. The calculated values of B_1 for both cases are given in Table IV.

One can see from Eqs. (24) and (27) that the relative size of the l -dependent intensity oscillation varies with n , the harmonic order. Thus, another test of our model is to apply it to another value of n . We have parametrized measurements of $(1-3\epsilon, 0, l)$ peaks ($l=1$ to 4) in terms of the coefficient B_3 , and the results for $T=80$ and 100 K are listed in Table IV. We then calculated values of B_3 using the parameter values already determined in the fits to the $n=1$ intensities. The calculated values are in very good agreement with the measurements. For reference, we have also included in Table IV calculated values of B_2 and B_4 .

Before leaving this section, it is of interest to consider the consequences of our model for the $n=2$ charge-order peaks. Measurements have not detected any intensity at positions $(2n \pm 2\epsilon, 0, l)$ with l even. Considering just the stacking contribution (that is, ignoring the structure factor due to the atomic displacement pattern within a single layer), we can calculate the relative intensities of even- l peaks compared to odd- l peaks. Using our results for $\epsilon = \frac{5}{18}$ gives a ratio of 2%, while for $\epsilon = \frac{2}{7}$ we obtain 8%. These relative intensities are still quite difficult to detect. For $\epsilon = \frac{1}{3}$ we calculate a ratio of 33%, which would be detectable except that the peak position overlaps with the second harmonic of $\mathbf{g}_{O(1)}$.

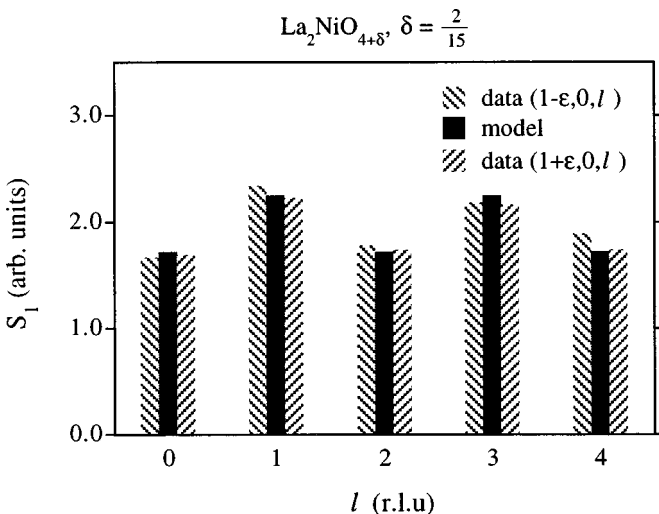


FIG. 8. Comparison of the structure factors $S_1(l)$ for the experimental data (corrected for Af^2) and least-squares fit for the first-harmonic intensities of the $\frac{5}{18}$ phase.

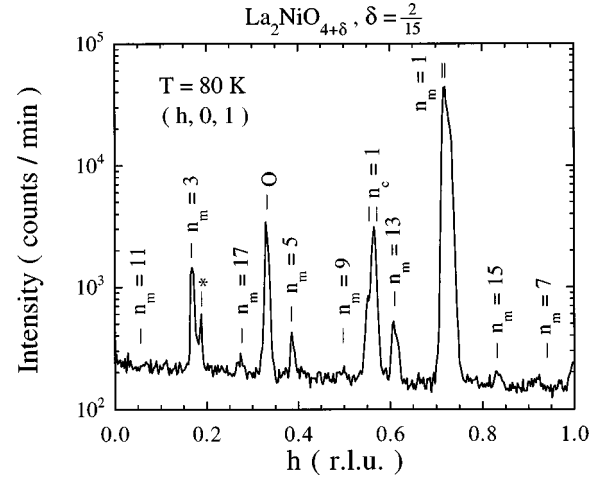


FIG. 9. Spectrum of higher order satellites in the $\frac{5}{18}$ phase at 80 K along $\mathbf{Q}=(h, 0, 1)$. The n th order magnetic satellites are labeled with subscript m , the ones due to charge order with c . An oxygen ordering peak is labeled O and one of undefined origin with (*).

VI. MAGNETIC HARMONIC SATELLITE SPECTRUM

Information on deviations from a sinusoidal modulation is contained in the relative intensities of the higher harmonic superlattice peaks. In particular, we are interested in the degree to which the spacing of the stripes deviates from perfect periodicity as well as the degree to which the charge is confined within narrow stripes. By reason of their greater absolute intensities, the magnetic harmonics are best suited for quantitative analysis.

For the $\epsilon = \frac{5}{18}$ phase found at 80 K, there are nine independent harmonics. Figure 9 illustrates the spectrum of higher-order magnetic and charge satellites found in a scan along $(h, 0, 1)$ for $0 \leq h \leq 1$. Because of the weakness of the higher harmonics, the intensity is plotted on a logarithmic scale. The n th order satellites of magnetic origin are denoted by the subscript m , while those due to charge order are indicated by the subscript c . An oxygen ordering peak at $(\frac{1}{3}, 0, 1)$ (labeled O) and an unexplained peak close to $n_m = 3$ (labeled *) are also recorded. (The latter very weak peak is probably due to a misaligned grain.) Because of insufficient cooldown time for this special scan, the first magnetic and charge satellites are split in two due to partial coexistence of the $\frac{5}{18}$ and $\frac{2}{7}$ phases. Higher-order contributions of the $\frac{2}{7}$ phase could not be observed in this scan.

In order to allow a quantitative analysis, separate measurements (following a more careful cool down) were performed to obtain integrated intensities for all independent magnetic harmonics. These were done at 80 and 100 K to characterize the $\frac{5}{18}$ and $\frac{2}{7}$ phases, respectively. All peaks in the range $\mathbf{Q}=(h, 0, 1)$ with $-1 < h < 1$ were measured, and values at $+h$ and $-h$ were averaged. The results, normalized to the intensity of the first harmonic, are listed in Tables VI and VII.

To model the harmonic intensities, we must start with a specific model of the spin density within a unit cell of the stripe pattern, such as the models shown in Sec. IV B. Within such a one-dimensional unit cell, if we number the sites with an integer index m and denote the spin on the m th site as S_m , the discrete Fourier transform of the spin arrange-

TABLE VI. Relative intensities of the n th order magnetic satellite peaks in the Q range ($h,0,1$) with $-1 < h < 1$ for $\epsilon = \frac{5}{18}$. Both observed and fitted values are listed.

n	$(I_n/I_1)_{\text{obs}}$ (%)	$(I_n/I_1)_{\text{calc}}$ (%)
3	1.70(21)	1.008
5	0.10(10)	0.168
7	0.10(7)	0.024
9	0.001(1)	0.136
11	0.001(1)	0.014
13	0.90(16)	0.642
15	0.10(3)	0.309
17	0.10(5)	0.121
R_w		0.47

ment corresponding to the n th harmonic is then

$$\bar{S}_n = \frac{1}{N} \sum_{m=0}^{N-1} S_m e^{-i\pi m} e^{-i2\pi n \epsilon m}, \quad (28)$$

where $N=36$ (14) for $\epsilon = \frac{5}{18}$ ($\frac{2}{7}$). The intensity of the n th-order satellite is given by

$$I_n \sim |\bar{S}_n|^2 |F_n|^2, \quad (29)$$

where F_n is given by Eq. (27). Because the measurements span a very small range of Q , the variation of the magnetic form factor and the Debye-Waller factor can be neglected.

We first consider the $\frac{2}{7}$ case, because it provides the opportunity to distinguish between three different models: (a) equally spaced stripes centered alternately on Ni and O rows, (b) stripes with alternating spacings centered only on Ni rows, or (c) stripes centered only on O rows. These three possibilities are illustrated in Eqs. (15)–(17), respectively. In each case, all spins are drawn with the same magnitude (unity), suggesting quite narrow charge stripes. To allow for some smoothing of the spin modulation, we treat the relative magnitude of a spin immediately adjacent to an O-centered stripe as a fitting parameter. Since no such sites occur in model (b), in that case alone we take the magnitude of the spins next to Ni-centered stripes as the fitting parameter. The intensities calculated with each of the models are presented in Table VII, and the fitted spin in each model is listed in Table VIII. Model (a), with equally spaced stripes, gives very good agreement with experiment, and the other two models are ruled out rather convincingly. As a further test of model (a), we allowed a second parameter, the size of the spin adjacent to a Ni-centered stripe, to vary, and found that it decreased only slightly, from 1.0 to 0.94, while the size of the spin next to an O-centered stripe remained unchanged.

To model the results for the $\frac{5}{18}$ phase we considered only a model similar to (a), with both Ni- and O-centered stripes, although in this case they are not all equally spaced. The fit gives the same value as in the $\frac{2}{7}$ case for the spin magnitude next to an O-centered stripe (see Table VIII). The calculated harmonic intensities are listed in Table VI. The R factor is somewhat worse than in the $\frac{2}{7}$ case, but we also have a substantially larger number of harmonics to fit. The quality of

TABLE VII. Same as previous table, but for $\epsilon = \frac{2}{7}$. The different models are described in the text.

n	$(I_n/I_1)_{\text{obs}}$ (%)	$(I_n/I_1)_{\text{calc}}$ (%)		
		Model (a)	Model (b)	Model (c)
3	0.81(19)	0.910	0.355	1.836
5	0.04(4)	0.051	0.063	0.217
R_w		0.13	0.56	1.42

the fit seems quite reasonable given the relative complexity of the structure and the possible systematic errors in measuring the very weak harmonics.

Given that the analysis of the magnetic harmonics indicates fairly narrow charge stripes, it is of interest to study the charge-order harmonics. The information obtained about the charge modulation is still indirect, because the neutrons are only directly sensitive to the induced atomic displacements. Furthermore, quantitative modeling is difficult because of the strong Q dependence of the structure factor, even for a single layer.⁸ Nevertheless, an attempt was made to detect higher harmonics. Since the lowest-order superlattice peaks for charge order correspond to $n=2$, the next harmonic is $n=4$. The strongest $n=2$ peak within the accessible Q range is at $(4-2\epsilon, 0, 1)$. Searching in the nearby region we found finite $n=4$ peaks at $(4-4\epsilon, 0, l)$ with $l=0$ and 2. At $T=8$ K the intensities of the latter two peaks, relative to the strong $n=2$ peak, are 1.4(7)% and 2.2(7)%, respectively.

VII. DISCUSSION

In the Landau model for coupled charge- and spin-density-wave order parameters,³⁴ there are two possible ordering scenarios. If, on cooling, the first-ordering transition is driven by the pure charge term in the free energy, then spin ordering will tend to occur at a lower temperature; otherwise, the spin and charge order will appear simultaneously. Our present results for the $\delta=0.133$ phase of $\text{La}_2\text{NiO}_{4+\delta}$ show that charge order appears first, consistent with the behavior found in $\text{La}_{2-x}\text{Sr}_x\text{NiO}_4$ (Refs. 4, 7, 9, 11, 36) and in $\text{La}_{1.6-x}\text{Nd}_{0.4}\text{Sr}_x\text{CuO}_4$ (Refs. 37, 38). Thus, it is the free energy associated with the charge alone that drives the ordering. Of course, one must keep in mind that the charge stripes would not be likely to form and order in the absence of the magnetic moments of the Ni ions.¹⁵ In the charge-ordered phase at $T > T_m$, the Ni spins remain strongly correlated, as demonstrated by inelastic neutron-scattering measurements reported elsewhere.³⁰

TABLE VIII. Values for the relative magnitude of the Ni spins adjacent to a domain wall obtained in fitting the relative intensities of the higher-order magnetic satellite peaks. Models (a), (b), and (c) are described in the text.

Model	Fitted reduction factor for $\langle S_{\text{Ni}} \rangle$ near DW	
	$\epsilon = \frac{2}{7}$	$\epsilon = \frac{5}{18}$
(a)	0.65(2)	0.66(6)
(b)	0.44(4)	
(c)	0.26(8)	

The exponential decrease of the charge-order peak intensity at high temperatures is unusual, but appears to be associated with a commensurability with the superlattice formed by the interstitial oxygens. This coupling, together with the simultaneous appearance of interstitial order and charge-stripe order as a function of δ , leads one to wonder whether the energy associated with the charge and spin correlations might influence the ordering of the interstitial oxygens. Perhaps this connection could be tested in a future experiment.

The first-order transition at T_m and the concomitant jump in I_{ch} are consistent with the generic Landau model.³⁴ The main feature not explained by that model is the temperature dependence of ϵ . The similarity of the series of lock-in transitions to what is observed in solutions of anisotropic next-nearest-neighbor Ising models^{39,40} suggests the importance of competing interactions. (Of course, it is likely that competing interactions are also responsible for the very existence of stripes in this system.⁴¹⁻⁴⁴) One relevant factor is the long-range part of the Coulomb interaction, which favors a uniform distribution of charge, and hence a large value of ϵ .^{9,42-44} A competing factor is the superexchange energy associated with antiferromagnetic Ni spins. This interaction favors wide magnetic domains, and therefore a small value of ϵ .^{42,45} The competition between these energies will depend on the relative magnitudes of the order parameters ρ and S , resulting in a temperature-dependent ϵ . The observation⁹ of a very similar temperature dependence (without the lock-ins) in $\text{La}_{2-x}\text{Sr}_x\text{NiO}_4$ with $x=0.225$, where the dopant ions are randomly distributed, demonstrates that this behavior does not require well ordered dopants.

The lock-in transitions provide evidence for some coupling to the lattice. We have explained how the values of ϵ observed at lock-in plateaus can be understood in terms of long-period commensurate structures. Only commensurate structures with relatively short periods can be stabilized at finite temperature. Between the plateaus entropy will tend to favor incommensurate structures.³⁹ The values of epsilon corresponding to observed commensurate structures may at first appear to be somewhat arbitrary rational fractions; however, it is interesting to note that they form the first levels of a Farey tree.^{45,46} A similar correspondence was observed previously by Shimomura, Hamaya, and Fujii⁴⁷ in an x-ray-diffraction study of commensurate-incommensurate transitions in the system $[\text{N}(\text{CH}_3)_4]_2\text{MCl}_4$, where $M=\text{Zn}, \text{Fe},$ and Mn . A Farey tree is constructed by evaluating a sequence of Farey mediants. Given two rational fractions, n'/n and m'/m , the Farey mediant is $(n'+m')/(n+m)$. Starting with the fractions $\frac{1}{4}$ and $\frac{1}{3}$ one obtains the tree shown in Fig. 10. The experimentally observed values of ϵ are marked. Farey-tree structures have also been noted in studies of the two-dimensional Falicov-Kimball model in regions of the phase diagram dominated by stripe configurations.⁴⁸

It was shown previously⁸ in a neutron-diffraction study of stripe order in a $\delta=0.125$ sample that the ordered Ni moments are quite large, with a maximum amplitude that is $>80\%$ of that observed in undoped La_2NiO_4 . Here we have shown that the observed intensities of magnetic harmonics are consistent with fairly narrow domain walls. These results, together with the poor conductivity of the nickelates in general, suggest that the dopant-induced holes are strongly localized within relatively narrow charge stripes. The weak-

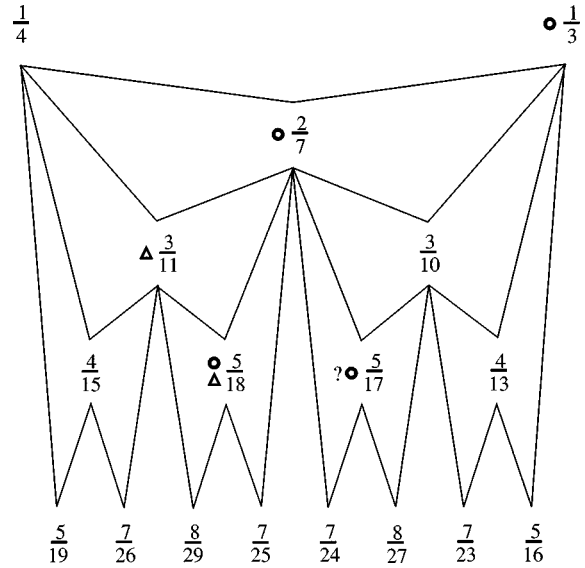


FIG. 10. Farey-tree composition rule for wave vectors (densities) between $1/4$ and $1/3$. The observed rational values for ϵ are marked by the symbols \circ and Δ for $\text{La}_2\text{NiO}_{4.133}$ and $\text{La}_2\text{NiO}_{4.125}$, respectively.

ness of the higher harmonics relative to the first harmonic peak occurs because of the small number of atomic sites between domain walls: the difference in harmonic intensity between a square wave and a sine wave is small when there are only a few lattice sites per period. It follows that the absence of strong higher harmonics in magnetic scattering studies of copper-oxide superconductors such as $\text{La}_{2-x}\text{Sr}_x\text{CuO}_4$ is not inconsistent with the existence of stripe correlations in those materials.

It is interesting to consider the change in character of the charge stripes with temperature. As we have shown elsewhere,²⁹ the charge stripes in the $\epsilon=\frac{1}{3}$ phase, above T_m , are centered on oxygen rows. From the analysis of the harmonic intensities, we have shown here that, in the $\epsilon=\frac{2}{7}$ phase, the charge stripes are half O centered and half Ni centered. Continuing to lower temperature, the domain walls become dominantly Ni centered. In fact, this shift of the stripes from O to Ni centered is correlated with the evolution of the magnetic order parameter. We have observed that, at least near the transition, the intensity of the first magnetic harmonic is proportional to the square of the quantity q defined by Eq. (9). One can easily show that $3q$ is equal to the density of Ni-centered stripes. The significance of this curious correlation is not clear.

Along with the shift in lattice alignment, we have argued that the charge density within the stripes must vary with temperature. It follows that the insulating nature of the material cannot be explained simply by invoking a Peierls transition in 1D half-filled stripes.¹⁵ Instead, it appears that the electronic localization must be understood in terms of interactions in the direction transverse to the stripes. While electron-phonon interactions are often discussed, the temperature dependence of ϵ makes it clear that purely electronic effects are more important than coupling to the lattice. It has been suggested previously^{49,50} that ‘‘magnetic confinement’’ effects are relatively strong in nickelates, especially when compared to cuprates. Perhaps this effect, associated

with the size of the transition-metal moments, is the most important feature distinguishing the nickelates from the cuprates.

VIII. SUMMARY

We have reported a detailed study of stripe ordering in a single crystal of $\text{La}_2\text{NiO}_{4+\delta}$ with $\delta = \frac{2}{15}$. On cooling, charge order occurs before magnetic order, although there is a substantial jump in the charge order parameter at the first-order magnetic transition. No clear charge-order superlattice peak decays exponentially with temperature. Below T_m , the value of ϵ decreases with temperature, exhibiting several lock-in transitions. A model in which each charge stripe is centered on either a row of Ni or O ions has been shown to be consistent with the l dependence of the magnetic peak

intensities and with the intensities of higher-order magnetic harmonic peaks. Modeling of the latter also indicates relatively narrow magnetic domain walls. With decreasing temperature the charge stripes are initially all centered on O rows, and then begin to shift to Ni rows below T_m , with Ni-centered rows dominating at low temperature.

ACKNOWLEDGMENTS

We gratefully acknowledge helpful discussions with V. J. Emery, S. A. Kivelson, and O. Zachar. The detailed examination of higher harmonic reflections was motivated by conversations with P. B. Littlewood. Enthusiastic encouragement from J. Zaanen is appreciated. Work at Brookhaven was carried out under Contract No. DE-AC02-76CH00016, Division of Materials Sciences, U.S. Department of Energy.

*Present address: Rodel Inc., 451 Bellevue Road, Newark, Delaware 19713.

¹J. Gopalakrishnan, G. Colsmann, and B. Reuter, *J. Solid State Chem.* **22**, 145 (1977).

²R. J. Cava *et al.*, *Phys. Rev. B* **43**, 1229 (1991).

³T. Strangfeld, K. Westerhold, and H. Bach, *Physica C* **183**, 1 (1993).

⁴C. H. Chen, S.-W. Cheong, and A. S. Cooper, *Phys. Rev. B* **71**, 2461 (1993).

⁵S.-W. Cheong *et al.*, *Phys. Rev. B* **49**, 7088 (1994).

⁶J. M. Tranquada, D. J. Buttrey, V. Sachan, and J. E. Lorenzo, *Phys. Rev. Lett.* **73**, 1003 (1994).

⁷V. Sachan *et al.*, *Phys. Rev. B* **51**, 12 742 (1995).

⁸J. M. Tranquada, J. E. Lorenzo, D. J. Buttrey, and V. Sachan, *Phys. Rev. B* **52**, 3581 (1995).

⁹J. M. Tranquada, D. J. Buttrey, and V. Sachan, *Phys. Rev. B* **54**, 12 318 (1996).

¹⁰K. Nakajima *et al.*, *J. Phys. Soc. Jpn.* **66**, 809 (1997).

¹¹S.-H. Lee and S.-W. Cheong, *Phys. Rev. Lett.* **79**, 2514 (1997).

¹²S. M. Hayden *et al.*, *Phys. Rev. Lett.* **68**, 1061 (1992).

¹³P. J. Brown *et al.*, *Physica B* **180&181**, 380 (1992).

¹⁴S. A. Kivelson and V. J. Emery, *Synth. Met.* **80**, 151 (1996).

¹⁵J. Zaanen and P. B. Littlewood, *Phys. Rev. B* **50**, 7222 (1994).

¹⁶X.-X. Bi *et al.*, *Phys. Rev. B* **42**, 4756 (1990).

¹⁷T. Ido, K. Magoshi, H. Eisaki, and S. Uchida, *Phys. Rev. B* **44**, 12 094 (1991).

¹⁸X.-X. Bi and P. C. Eklund, *Phys. Rev. Lett.* **70**, 2625 (1993).

¹⁹D. A. Crandles, T. Timusk, J. D. Garret, and J. E. Greedan, *Physica C* **216**, 94 (1993).

²⁰P. Calvani *et al.*, *Phys. Rev. B* **54**, R9592 (1996).

²¹T. Katsufuji *et al.*, *Phys. Rev. B* **54**, R14 230 (1996).

²²J. Rodríguez-Carvajal, M. T. Fernández-Díaz, and J. L. Martínez, *J. Phys.: Condens. Matter* **3**, 3215 (1991).

²³S. Hosoya *et al.*, *Physica C* **202**, 188 (1992).

²⁴D. E. Rice and D. J. Buttrey, *J. Solid State Chem.* **105**, 197 (1993).

²⁵H. Tamura, A. Hayashi, and Y. Ueda, *Physica C* **216**, 83 (1993).

²⁶J. M. Tranquada *et al.*, *Phys. Rev. B* **50**, 6340 (1994).

²⁷I. Yazdi *et al.*, *Chem. Mater.* **6**, 2078 (1994).

²⁸K. Yamada *et al.*, *Physica C* **221**, 355 (1994).

²⁹J. M. Tranquada, P. Wochner, A. R. Moodenbaugh, and D. J. Buttrey, *Phys. Rev. B* **55**, R6113 (1997).

³⁰J. M. Tranquada, P. Wochner, and D. J. Buttrey, *Phys. Rev. Lett.* **79**, 2133 (1997).

³¹J. Hubbard, *Phys. Rev. B* **17**, 494 (1978).

³²P. Bak and R. Bruinsma, *Phys. Rev. Lett.* **49**, 249 (1982).

³³J. E. Lorenzo, J. M. Tranquada, D. J. Buttrey, and V. Sachan, *Phys. Rev. B* **51**, 3176 (1995).

³⁴O. Zachar, S. A. Kivelson, and V. J. Emery, *Phys. Rev. B* (to be published).

³⁵V. L. Pokrovsky and G. V. Uimin, *J. Phys. C* **11**, 3535 (1978).

³⁶A. P. Ramirez *et al.*, *Phys. Rev. Lett.* **76**, 447 (1996).

³⁷J. M. Tranquada *et al.*, *Nature (London)* **375**, 561 (1995).

³⁸J. M. Tranquada *et al.*, *Phys. Rev. B* **54**, 7489 (1996).

³⁹P. Bak and J. von Boehm, *Phys. Rev. B* **21**, 5297 (1980).

⁴⁰M. E. Fisher and W. Selke, *Phys. Rev. Lett.* **44**, 1502 (1980).

⁴¹M. Seul and D. Andelman, *Science* **267**, 476 (1995).

⁴²S. A. Kivelson and V. J. Emery, in *Strongly Correlated Electronic Materials: The Los Alamos Symposium 1993*, edited by K. S. Bedell *et al.* (Addison-Wesley, Reading, MA, 1994), pp. 619–656.

⁴³U. Löw, V. J. Emery, K. Fabricius, and S. A. Kivelson, *Phys. Rev. Lett.* **72**, 1918 (1994).

⁴⁴L. Chayes *et al.*, *Physica A* **225**, 129 (1996).

⁴⁵O. Zachar (private communication).

⁴⁶G. H. Hardy and E. M. Wright, *An Introduction to the Theory of Numbers* (Clarendon, Oxford, 1954), p. 23.

⁴⁷S. Shimomura, N. Hamaya, and Y. Fujii, *Phys. Rev. B* **53**, 8975 (1996).

⁴⁸G. I. Watson and R. Lemanski, *J. Phys.: Condens. Matter* **7**, 9521 (1995).

⁴⁹V. I. Anisimov, M. A. Korotin, J. Zaanen, and O. K. Andersen, *Phys. Rev. Lett.* **68**, 345 (1992).

⁵⁰J. Loos and H. Fehske, *Czech. J. Phys.* **46**, 1879 (1996).